JOURNAL OF GEOPHYSICAL RESEARCH, VOL. 111, E12008, doi:10.1029/2006JE002712, 2006

Long-period seismology on Europa: 2. Predicted seismic response

M. Panning,[1,2] V. Lekic,[1] M. Manga,[3] F. Cammarano,[1] and B. Romanowicz[1]

Received 6 March 2006; revised 15 September 2006; accepted 3 November 2006; published 29 December 2006.

[1] Previous studies have documented the potential for using relatively short-period body waves and intermediate-period surface waves to explore the structure and tectonics of Europa. We show that long-period measurements (0.001 to 0.1 Hz) may have large amplitudes of displacement (millimeters to centimeters) and are potentially measurable from orbit without requiring a lander. To accurately model the long-period response of Europa, we use normal modes calculated from physically self-consistent models of Europa's structure developed in part 1 (Cammarano et al., 2007). On the basis of the geometry of observed faults, we estimate that faulting events of magnitude 5 or larger may occur regularly. Synthetic seismograms show that long-period displacement measurements with millimeter accuracy could detect current tectonic activity and determine the thickness of Europa's ice shell, and confirm the presence of a subsurface ocean. Determination of deeper structure with seismic measurements, however, is more challenging in the presence of a global liquid ocean, which acts to decouple deeper seismic energy from the surface.

Citation: Panning, M., V. Lekic, M. Manga, F. Cammarano, and B. Romanowicz (2006), Long-period seismology on Europa: 2. Predicted seismic response, *J. Geophys. Res.*, *111*, E12008, doi:10.1029/2006JE002712.

1. Introduction

[2] Seismological observations provide unparalleled capability for studying planetary interiors. While seismological studies of the Earth and, to a lesser extent, the Earth's Moon have placed strong constraints on the internal structure and dynamics of these bodies, the absence of seismic measurements on other planetary bodies has stymied analysis of their detailed structures. There are a wide variety of internal compositions and structures hinted at by recent exploration of the Jovian and Saturnian systems. In order to inform future mission design, it is important to determine what observations hold potential for answering outstanding questions concerning planetary interiors.

[3] Physically consistent models of planetary bodies, constrained by moment of inertia measurements and by well-characterized elastic and anelastic properties of relevant minerals, make possible the study of the seismic response of planetary bodies, even when seismic measurements are not yet available. In particular, physically consistent models of Jupiter's moon Europa developed in our companion paper [*Cammarano et al.*, 2007] (hereinafter referred to as Paper 1) allow us to explore which seismic measurements on Europa have the potential to answer the many outstanding questions about its structure and current thermal state. Accurate predictions of the seismic response of Europa to various proposed sources are essential for planning missions aimed at taking seismic measurements.

[4] The dominantly water ice surface of Europa is highly fractured. In combination with the relatively young age of approximately 60 Myrs derived from crater counts [*Zahnle et al.*, 2003], this suggests recent tectonic activity. Therefore the first question we can pose for seismological measurements on Europa is whether there is any current tectonic activity. If there is, we would like to know the nature of the seismic sources. Can we detect ice-cracking events, such as tensile cracks [*Lee et al.*, 2003], normal faulting [*Nimmo and Schenk*, 2006], or motion on one of the many observed strike-slip faults [*Schenk and McKinnon*, 1989; *Hoppa et al.*, 2000]? Can we observe deeper seismic events in the rocky portion of Europa analogous to the deep quakes observed on Earth's moon [*Nakamura*, 1978]?

[5] Magnetic induction measurements [*Kivelson et al.*, 2000] also imply the presence of a liquid ocean beneath the solid ice shell. Seismic measurements should be able to confirm or disprove the presence of this liquid ocean, and determine the thickness of the ice shell. Characterizing the depth to Europa's ocean would have important implications for any mission aimed at penetrating the ice shell.

[6] Seismic measurements may also make it possible to answer questions about the deeper structure. Mass and moment of inertia measurements from the Galileo mission place broad constraints on the radial structure of Europa. These suggest that it is differentiated with an ice/water layer, a rocky layer, and a denser core [e.g., *Anderson et al.*, 1998], but seismic measurements could better constrain

[1]Berkeley Seismological Laboratory, University of California, Berkeley, Berkeley, California, USA.
[2]Now at Department of Geosciences, Princeton University, Princeton, New Jersey, USA.
[3]Department of Earth and Planetary Science, University of California, Berkeley, Berkeley, California, USA.

0148-0227/06/2006JE002712$09.00

the radii of these divisions and therefore the chemistry and thermal state of the interior.

[7] Some work has already been carried out on the predictions of relatively high-frequency body waves [*Lee et al.*, 2003] and intermediate-frequency surface waves [*Kovach and Chyba*, 2001], but including the long-period response and considering the full range of expected internal structures provides a complementary approach for answering the outstanding questions, and for overcoming some of the challenges that might be faced in obtaining the body-wave measurements. In fact, obtaining suitable measurements poses many technical challenges. Installing a seismometer on the surface requires a lander mission, and the high radiation due to Jupiter's magnetic field places limits on the operational lifespan of surface instruments. However, as Europa has little atmosphere, orbital-based measurements of ground displacement might be possible if the ground motion is large enough.

2. Calculation of the Broadband Seismic Response

[8] In order to predict the seismic observations, we must first know the radial structure of Europa. To this end, we developed a suite of physically consistent models by considering different initial core and mantle compositions, as well as a two end-member thermal profiles which account for whether the rocky interior experiences significant tidal heating or not. The methodology is discussed in detail in Paper 1, but, in summary, we produce a range of models consistent with the mass and moment of inertia constraints, as well as mineral physics constraints which are well known for the relatively small pressure range of Europa's interior.

[9] Given a radial model of Europa's structure, we can calculate the normal modes of the spherical body. This is accomplished using a code derived for the specifics of Europa models from the well-developed MINOS code [*Woodhouse*, 1988]. Seismograms for any proposed source and receiver configuration can then be modeled using normal mode summation, which models the complete broadband seismic wavefield. These mode catalogs are calculated for the entire range of models, allowing comparisons of seismic response between different models. These comparisons are then used to determine what measurements need to be made to discriminate among possible physical models of Europa.

3. Expected Sources of Seismic Energy

[10] Europa has many surface features (ridges, bands, cycloids, etc.) indicative of tectonic activity in the past 60 million years. Because of the eccentricity of Europa's orbit around Jupiter, there are significant tidal stresses in the ice shell. Estimates of the magnitude of tidal stress range from 40 kPa [*Hoppa et al.*, 1999] to 100 kPa [*Leith and McKinnon*, 1996; *Greenberg et al.*, 1998]. Additionally, although Europa's rotational period is nearly synchronous with its orbit around Jupiter, there is evidence of nonsynchronous rotation [*Geissler et al.*, 1998], which would cause stresses approximately a factor of 30 larger over longer timescales [*McEwen*, 1986].

3.1. Tensile Cracks

[11] In extensional regimes, owing to tidal stresses, it is likely that tensile cracks will open, potentially on a diurnal basis [*Lee et al.*, 2003]. Tensile cracks can be expected to open to depths where the forcing stress is compensated by the pressure due to the overburden. Given Europa's gravity ($g = 1.3$ m/s^2) and the density of ice, we can expect the diurnal stress to open cracks to a maximum depth of 50–100 m. Assuming a square crack 100m on a side, the model of *Lee et al.* [2003] suggests an opening width of 1–2 mm, which produces a seismic moment of $\sim 2 \times 10^{11}$ Nm [*Aki and Richards*, 2002]. This corresponds to an event with moment magnitude $M_W \sim 2$. While this may be sufficient to produce low-amplitude and high-frequency data measurable with a surface seismometer installation, it is unlikely to produce displacements measurable from orbit. However, more recent work suggests that the theory outlined above, which assumes cracks in an elastic half-space, may underestimate cracking depths when the finite thickness of the ice shell is considered [*Lee et al.*, 2005]. Therefore deeper cracking may occur diurnally, thus producing larger events.

[12] The larger stress from nonsynchronous rotation should also allow deeper cracking on the order of 1–3 km. This depth is roughly consistent with estimates of the brittle-ductile transition in the ice shell [*Pappalardo et al.*, 1999; *Ruiz*, 2005; *Billings and Kattenhorn*, 2005]. Using the *Lee et al.* [2003] model, we would predict opening widths of approximately 10 cm for these larger cracks, producing a quake of $M_W \sim 4$.

3.2. Normal Faults

[13] *Nimmo and Schenk* [2006] identify two normal faults in a region where high resolution topography is available from Galileo measurements. The fault scarps have lengths of 11 and 30 km. The two faults are modeled to have total displacements of 200 m and 600 m. *Nimmo and Schenk* [2006] estimate quakes of $M_W = 5.3$ on the larger fault assuming it ruptures to the brittle ductile transition and releases a critical strain of 0.05% based on terrestrial analogues, and the shear modulus of the near-surface ice is reduced from unfractured ice by a factor of 10 due to the presence of an extensive regolith as suggested by other studies [*Nimmo et al.*, 2003; *Eluskiewicz*, 2004; *Lee et al.*, 2005]. If the regolith is not as well-developed as assumed and the event ruptures ice with a shear modulus closer to that of pure unfractured ice at the pressure and temperature conditions of Europa's near-surface, the expected magnitude increases to $M_W \sim 6$. While we have no direct information on the frequency of such events, the total displacement of the modeled fault suggests $\sim$400 events have occurred on this fault, although the age of the feature is unknown [*Nimmo and Schenk*, 2006]. It is also not unreasonable to expect that many more such faults exist in regions where the Galileo data lacks the resolution to discover them, so it is possible that such an event could occur during a mission.

3.3. Strike-Slip Faults

[14] The surface of Europa shows many features with resolvable strike-slip motion. Strike-slip faults greater than 20 km in length have been observed in Voyager data

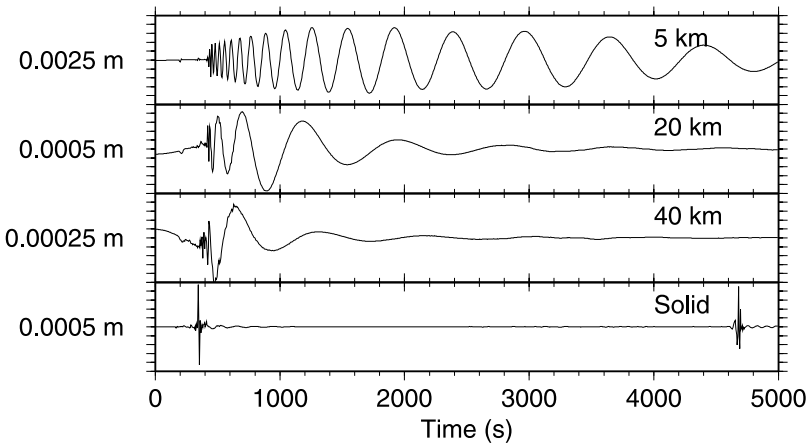

Figure 1. Synthetic displacement seismograms at a distance of 25° (680 km) from the $M_W = 5$ normal event. Seismograms are calculated for the low-attenuation cold chondritic model with ice shell thicknesses (from top) of 5, 20, 40, and a solid 137 km thick ice layer model. Seismograms are band-pass filtered between 0.001 and 0.1 Hz. The maximum amplitude for each panel is shown to the left of the panel.

[*Schenk and McKinnon*, 1989], and more recent studies of Galileo data [*Hoppa et al.*, 2000] have imaged more than a hundred strike-slip faults with lengths ranging from a few kilometers to many hundreds of kilometers, and total displacements ranging from hundreds of meters to as much as 83 km [*Sarid et al.*, 2002]. The longest fault, Astypalaea Linea, is 800 km long, comparable to the San Andreas fault system on Earth. One model put forth for the mechanism for these faults is diurnal "walking" [*Hoppa et al.*, 1999], which suggests that these faults are activated during the tensile portion of tidal stressing and slip freely while unclamped, allowing shear motion. The return motion is inhibited during the compressional portion of the tidal cycle and net displacement is achieved through anelastic deformation. This model correctly predicts the hemispherical distribution of right and left-lateral faulting. While this model is developed assuming either a state of free slip or locked fractures, it is likely that frictional sliding would occur when such a fracture is unclamped. Given the extensive length of many of the faults that are modeled to activate on a diurnal basis, it might be reasonable to observe an event that ruptures a 20 km length segment extending down to a depth of 1 km. Assuming the same slip scaling as for the normal faults discussed above, and the shear modulus of unbroken ice, this would produce a $M_W = 5.2$ event. An upper bound estimate for strike-slip events that might occur could be a 100 km long rupture to 3 km depth, which would produce an $M_W = 6.4$ event, although it would of course be possible to generate even larger events using the geometry of Astypalaea Linea, the largest observed surface strike-slip feature.

3.4. Deeper Events

[15] Apollo seismic data have shown that deep quakes occur in clusters on Earth's moon due to tidal stresses [*Lammlein*, 1977; *Nakamura*, 1978]. The largest of these clusters has events with moments of $\sim 5 \times 10^{13}$ Nm ($M_W \sim 3$). Because tidal stresses on Earth's moon are only ~5 kPa [e.g., *Minshull and Goulty*, 1988], it might be reasonable to expect analogous but larger events in Europa's rocky mantle.

4. Synthetic Seismograms

[16] Using the calculated normal mode catalogs and a predicted seismic source process, we can now compute synthetic seismograms at any distance from the source. The seismograms presented here assume a $M_W = 5$ (seismic moment of 3.94×10^{16} Nm) normal faulting source, as proposed by *Nimmo and Schenk* [2006]. For simplicity, we used a dip-slip event with a 45° dip and 90° rake. We computed all modes up to 0.1 Hz, and then band-pass filtered the seismograms with corner frequencies at 12 and 800 seconds period, and cut-off frequencies at 10 and 1000 seconds period. Higher-frequency data, used for measurements of body wave travel times and shorter-period Love wave dispersion, have been discussed in the literature before [*Lee et al.*, 2003; *Kovach and Chyba*, 2001], but the lower-frequency data discussed here can be a complementary data set, possibly with greater potential for orbital observation. Seismic displacement, which may be measured by orbital laser range-finding approaches, is larger for lower frequencies. The surface wave energy, which dominates at lower frequencies, also decays less rapidly with distance due to 2-D geometric spreading on the surface rather than the 3-D geometric spreading of body waves, meaning that observations should be possible on a larger portion of the surface for a given event. Finally, the Rayleigh wave energy we model can be measured on the vertical component, suitable for line-of-sight orbital measurements.

[17] Because the candidate event is shallow (hypocentral depth of 300 m), the seismograms are dominated by energy from the fundamental mode branch (Figure 1). These modes are trapped in the ice shell and therefore have little to no sensitivity to deeper structure. For this reason, we only choose to show seismograms for the chondritic mantle model, as it is visually indistinguishable from the pyrolitic mantle model. The dominant control on the character of the seismograms is the ice shell thickness. For thinner ice

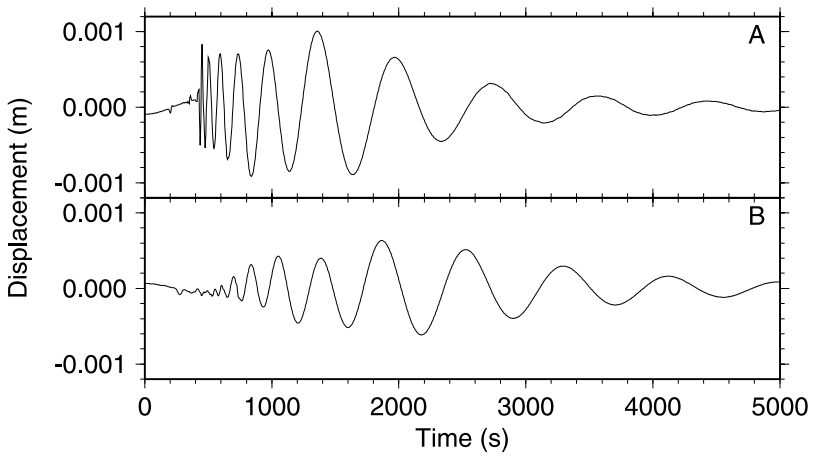

Figure 2. Synthetic displacement seismograms for same event-station configuration and frequency band pass as Figure 1 for (a) a low-attenuation model and (b) a high-attenuation model, both with ice shell thickness of 10 km.

shells, the surface wave train is very dispersive, with lower-frequency energy significantly delayed relative to the higher-frequency surface wave arrivals. Thicker ice shell models, however, are characterized by much more pulse-like surface wave arrivals.

[18] While the mantle composition has little impact on the observed seismograms, there is impact on the attenuation structure based on the choice of a hot or cold thermal profile. As there is little empirical constraint on the pressure and temperature dependence of seismic attenuation in ice,

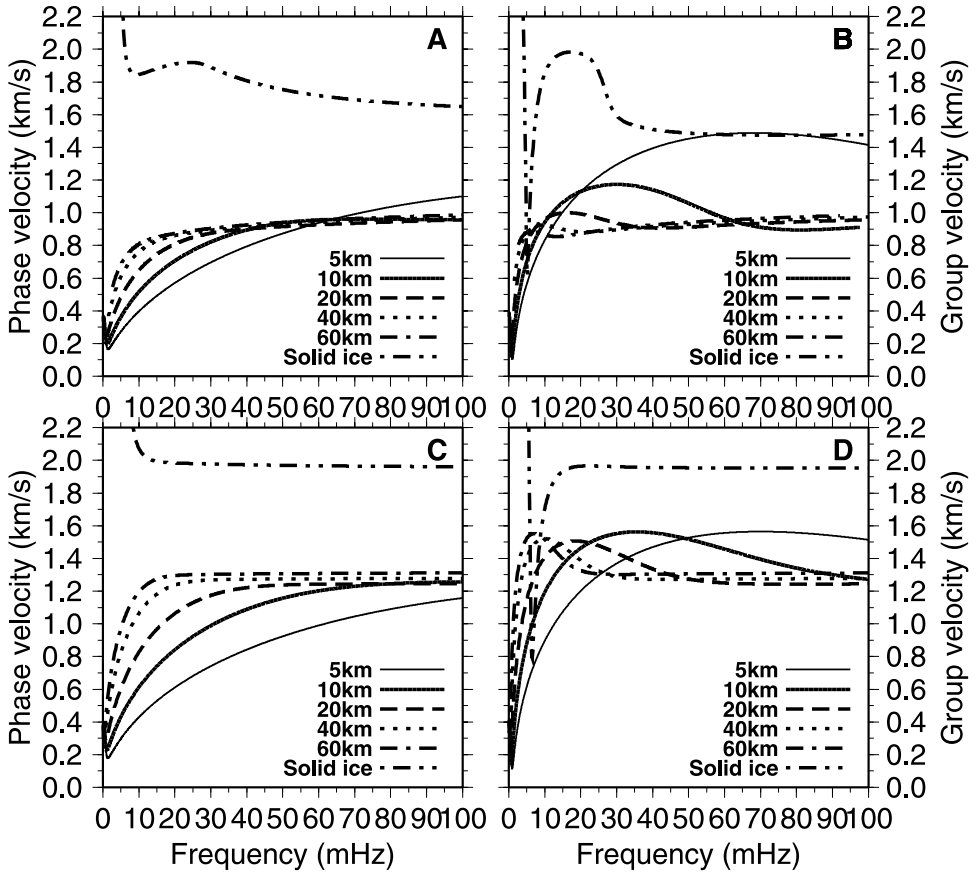

Figure 3. Theoretical (a and c) phase and (b and d) group velocity dispersion curves for fundamental mode Rayleigh waves for chondritic models for ice shells ranging from 5 to 60 km in thickness as well as the all-solid ice layer model calculated for (a and b) high-attenuation and (c and d) low-attenuation end-member models.

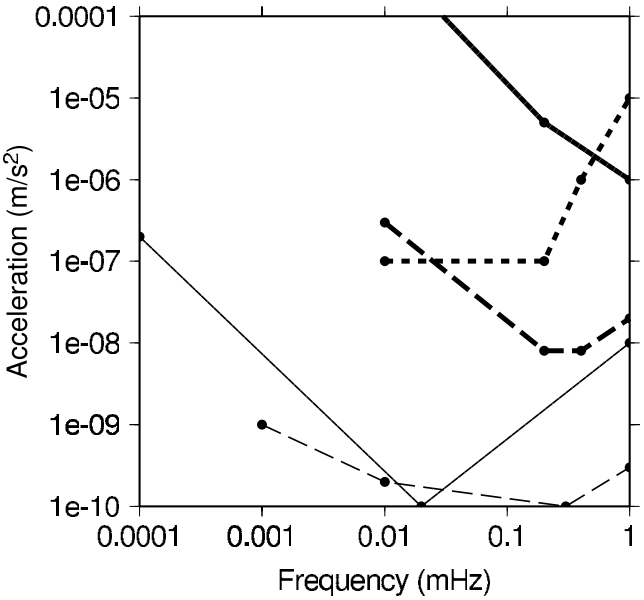

Figure 4. Acceleration sensitivities for previous and proposed planetary seismometers. Shown are the Viking seismometer (thick solid), the Mars96-Optimism instrument (4 samples/sec mode in thick long-dashed and 0.25 samples/sec mode in thick short-dashed), the Apollo LP (thin solid), and Netlander VBB (thin dashed).

we considered two cases, which differed through the choice of homologous temperature scaling relationship (Paper 1). Anelastic attenuation can be quantitatively described by the quality factor Q, which is a dimensionless measure of the energy lost (to friction and nonreversible deformation) per cycle of a seismic wave,

$$\frac{1}{Q} = -\frac{\Delta E}{2\pi E}, \tag{1}$$

where E is the peak strain energy and $-\Delta E$ is the energy lost in each cycle [*Aki and Richards*, 2002]. Materials with low Q are therefore highly attenuating, and high Q materials exhibit little attenuation. Figure 2a shows seismograms for a cold profile, using a value of 30 for the homologous temperature scaling parameter (Paper 1) which leads to the highest Q estimates, while Figure 2b shows the hot case with the scaling parameter assumed to be 22, which gives the lowest Q values for the same shell thickness of 10 km. While both models reach low Q values in the convecting regions of the ice shell, the high-attenuation choice reaches extremely low values less than 10, while the low-attenuation model Q never drops below 30. The high-attenuation model causes significant reduction of amplitudes of the earlier-arriving higher-frequency data, and some noticeable phase delay for the lower-frequency energy. Since the peak displacement amplitude occurs for low frequencies, the peak time-domain amplitude for the whole frequency band is only reduced by ~20%, although the reduction is more pronounced at higher frequencies.

[19] Quantitatively, we can explain the dispersive character of the seismograms by the theoretical phase and group velocity curves of the fundamental mode branch extracted from the mode catalog calculated for each model (Figure 3). For wavelengths less than the ice shell thickness, the surface wave is nearly nondispersive, and is similar to a Rayleigh wave in a homogeneous half-space. Because there is still some interaction with the finite thickness of the ice shell, there is a reduction of the Rayleigh wave velocity relative to the half-space model that is greater for the thinner ice shell models than for the thicker models. Below this frequency, the fundamental mode transitions to a flexural mode. The

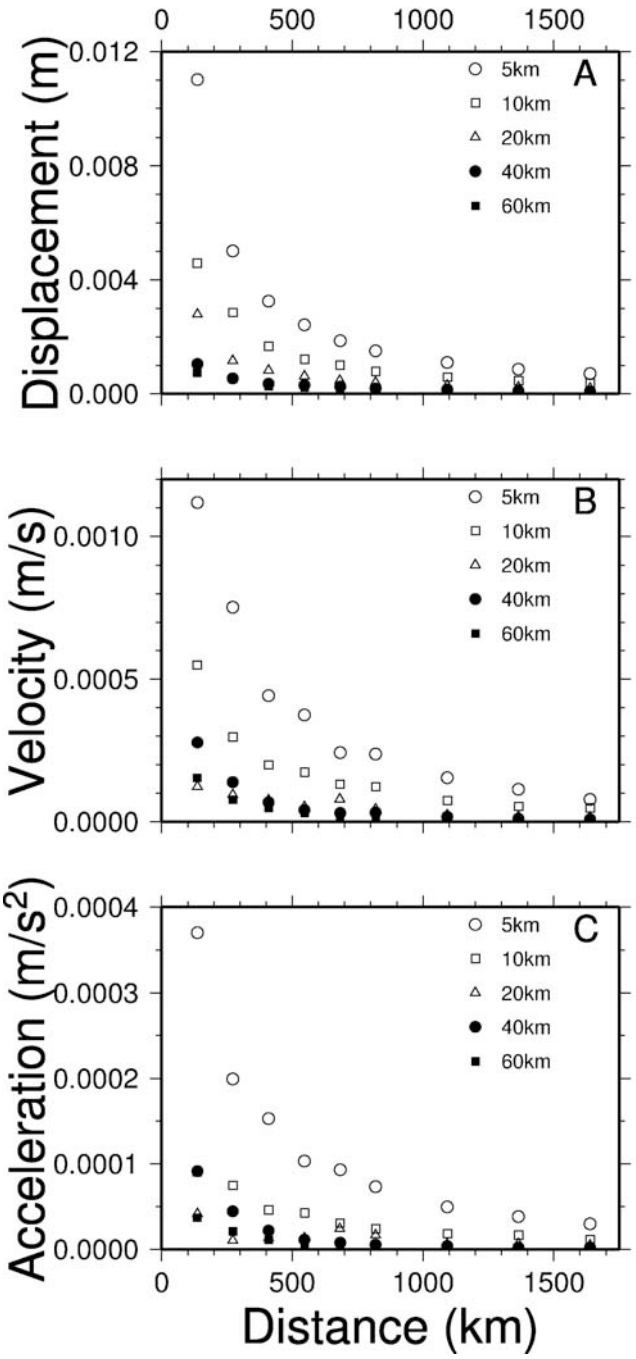

Figure 5. Peak amplitude in (a) displacement, (b) velocity, and (c) acceleration in the first orbit Rayleigh wave as a function of distance for models with ice shell thicknesses ranging from 5 to 60 km.

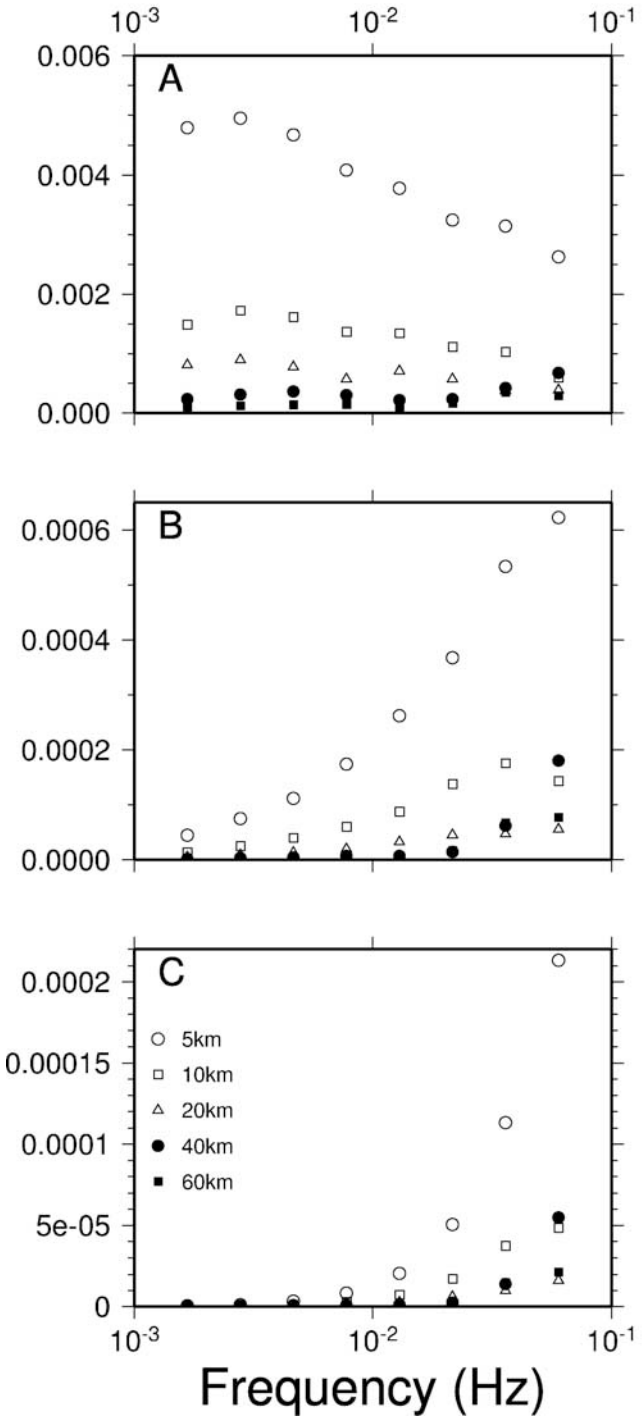

Figure 6. Peak time domain amplitude in (a) displacement, (b) velocity, and (c) acceleration in the first 3800 seconds of seismograms 5° (137 km) from the source after narrow band filtering about central frequencies between 0.001 and 0.1 Hz for models with ice shell thicknesses ranging from 5 to 60 km.

analytical expression for the dispersion of a flexural mode in a floating ice sheet is equivalent to that of a bending mode in an infinite plate, modified by the density ratio of the ice to the underlying water [*Press and Ewing*, 1951]. In this expression, the phase velocity is proportional to the wave number, which introduces a dispersion where the phase velocity is proportional to the square root of frequency, and the group velocity is twice the phase velocity. For the 5 km thick ice shell model, the frequency band of the synthetic seismograms is dominated by this flexural mode, and therefore very strong dispersion can be observed. For the thickest ice shell models, the frequency band is dominated by the Rayleigh wave, and is nearly nondispersive. The high-attenuation end-member models (Figures 3a and 3b), however, also have a significant anelastic dispersion slope due to the very low Q values in the hot part of the ice shell. In this end-member case, the group velocity peak associated with the transition to the flexural mode is less pronounced for thick ice shells.

5. Measurement Requirements

[20] Whether seismic measurements obtained from a mission to Europa are able to answer the outstanding scientific questions posed in the introduction depends on the sensitivity of the deployed instruments and the level of tectonic activity on Europa. For surface installations, there is sensitivity information available for many previous and proposed planetary surface seismometers [*Lognonné and Mosser*, 1993; *Lognonné et al.*, 2000; *Kovach and Chyba*, 2001] (Figure 4) and the Apollo LP, the Mars96 OPTIMISM which did not land, and the proposed Mars Netlander VBB instruments all have very good sensitivity in the frequency range proposed here. While the Apollo LP instrument probably has significantly too large mass and power requirements for any Europa mission (>11 kg and 4W, respectively), both the Mars96 Optimism [*Lognonné et al.*, 1998] and Netlander VBB [*Lognonné et al.*, 2000] instruments have mass less than 2 kg, and the Mars96 Optimism instrument was also designed for very low power consumption (<70 mW), while the Netlander VBB also had power consumption less than 1W. For an orbital measurement, the sensitivity will be lower, but the actual value will depend on many factors of mission design, such as the aperture of the optics used, the orbital altitude, and onboard noise sources. If there are $M_W \sim 5$ ice shell events observable during the course of a mission, then we can use our synthetic seismograms to directly determine the sensitivity and frequency characteristics that need to be observed in order to use the seismic data, regardless of whether observations are made at the surface or from orbit, or whether the measurement method is primarily sensitive to ground displacement, velocity, or acceleration.

[21] To inform mission design, we have computed the peak ground displacements, velocities, and accelerations as a function of ice shell thickness and angular distance from source ranging from 5° to 60° (~135–1640 km) (Figure 5). To further define the frequency characteristics of the observed signals, we also computed the peak time domain values after narrow band-passing the signals with cosine taper filters centered on frequencies from 0.001 to 0.1 Hz (Figure 6). We note here that for the 40 and 60 km thick ice shells in both attenuation models, the energy is somewhat reduced above 70 mHz, due to rejection of some high-frequency modes that were not well-resolved by the normal mode code. The peak values are strongly dependent on the

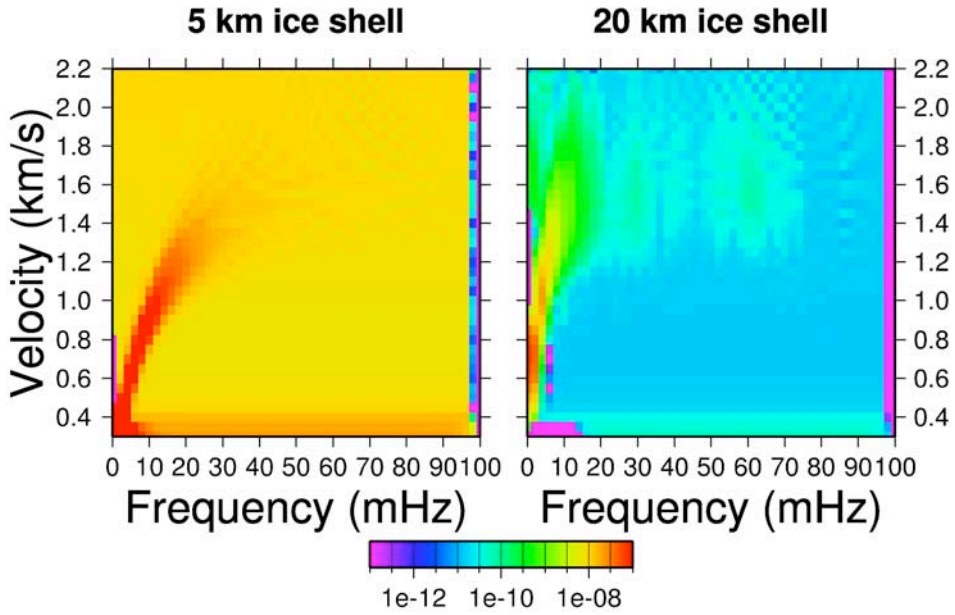

Figure 7. MFT output of squared data envelope after narrow band filtering of data 60° (1640 km) from the source calculated in models with a 5 km and 20 km thick ice shell. The color scale at each point corresponds to the amplitude of the squared envelope of the displacement record at the arrival time predicted by the velocity on the y axis and filtered at the center frequency on the x axis. The data include noise calculated from 20 randomly distributed events with magnitudes between 2 and 3.

ice shell thickness. For ice shells thinner than 20 km, there is considerable amplification as the ice shell becomes progressively thinner. Interestingly, the broadband amplitudes are generally smallest for the 20 km thick ice shell for velocity and acceleration measurements, but increase for thicker ice shells because the decreased dispersion leads to constructive stacking rather than the energy being dispersed across a broader frequency band. It is important to note that the frequency band controlling the peak amplitude is very different for displacement seismograms than for velocity or acceleration. For acceleration, the largest amplitudes are for periods shorter than 50 seconds, and therefore surface waves with wavelengths less than 70 km, comparable with the observed spacing of tectonic features at the surface. This may be problematic for our normal-mode synthetics which assume spherical geometry. For the highest-frequency data discussed here, there may also be complications owing to the finite dimensions of the faulting event in space and time, which are not modeled by the point source used for our synthetics. For seismic waves with frequencies greater than 70 mHz, observed data would be affected by the 20 km length of the modeled event, as well as the 10 seconds of source duration. Displacement peak amplitudes, however, are due to waves with periods greater than 200 seconds, therefore with wavelengths much greater than the observed fractures and the finite dimensions of the event.

[22] For displacement measurements of events of this size, where these longer-period surface wave signals have the greatest advantage over higher-frequency body wave approaches, any instrument needs to have at least millimeter-scale accuracy from periods ranging from 10 to 500 seconds to have a reasonable chance of observing seismic signals, although much larger signals might be observed if Europa has a thin ice shell, or if the measurements are obtained very near a seismic source. If no events as large as $M_W \sim 5$ occur during the time span of a mission, the signal amplitudes will scale linearly with seismic moment in this frequency band, as the periods of these signals will likely be longer than event source time functions for all events of this size and smaller.

6. Potential for Answering Questions

[23] In the scenario described above, determining whether Europa's ice shell is currently tectonically active is simply a matter of having instruments sensitive enough to measure the signal. Of course, it would be preferable to also determine the location and mechanism of any event. This would give us further information on the driving forces of the tectonic events. Ideally this could be achieved with multiple surface seismometer installations, but this is, of course, an extreme technical challenge given mission payload limitations, and the radiation endured by any instrument due to Jupiter's magnetic field. It is also possible to determine location and mechanism using waveform modeling with one very high-quality 3 component broadband instrument [e.g., *Pasyanos et al.*, 1996], although this requires adequate knowledge of the seismic structure between source and receiver, which would be challenging with a limited data set.

[24] Uniquely determining the ice shell thickness would also be easier using multiple stations, either distributed across the surface or in a small array. In this case, we could locate the event, thus allowing direct determination of surface wave group and phase velocities. While this may not be feasible for a lander-based mission, it may be possible to determine the propagation velocity and direction

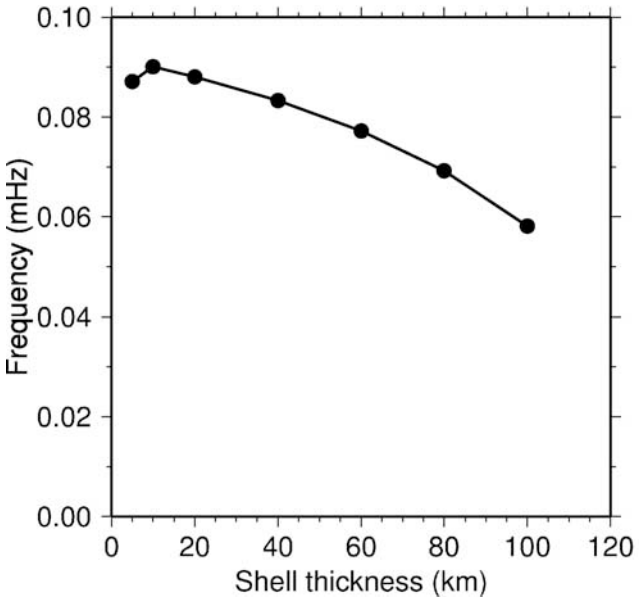

Figure 8. Frequency of mode ${}_0S_2$ (mHz) as a function of shell thickness.

of seismic energy using multiple aperture orbital instruments using small aperture array techniques [e.g., *Pedersen et al.*, 2003] or other processing of large footprint observations. Any method which can extract frequency-dependent phase and/or group velocity across this frequency band should be able to give a good estimate of ice shell thickness given the strong sensitivity. With a single point measurement, however, it still may be possible to determine ice shell thickness, even in the absence of a known source location. For example, the data can be processed using the Multiple Filter Technique (MFT) [*Dziewonski et al.*, 1969]. If the distance from the source is known, this approach can extract group velocity dispersion curves from a single measurement (Figure 7). If, however, the location is unknown, the shape of the dispersion curve can still be obtained, although the actual values of group velocity as a function of frequency would not be determined. However, the transition from Rayleigh mode propagation to flexural mode propagation leads to a distinctive peak in the group velocity curve which has a frequency dependent on the ice shell thickness. This means that a technique which can adequately resolve the shape of the group velocity curve from a single measurement, such as the MFT, can give a good estimate of ice shell thickness, even in the absence of location and absolute velocity information. The error in this estimation becomes larger for thicker ice shells, as the frequency of this peak changes little for thicknesses greater than 40 km. As mentioned earlier, this peak is also less pronounced for thicker ice shells in the presence of very high seismic attenuation (Figure 3). The dispersion curve, however, changes significantly in the absence of a liquid ocean layer (Figure 3), meaning this approach should still be able to reliably differentiate between a thick ice shell, and an ice layer extending all the way down to the rocky mantle.

[25] In theory, a complementary tool for determining ice shell thickness could be measurements of the frequency of mode ${}_0S_2$, the "football" mode, which is the gravest mode with significant surface deformation both in the Earth and Europa. The frequency of this mode is relatively constant for ice shells thinner than 20 km at about 0.09 mHz. It begins decreasing more rapidly as the ice shell thickens which could be diagnostic (Figure 8). However, if there is no liquid layer, the mode's frequency increases to 1.26 mHz. It should be noted, though, that all of these predictions are made for the lower-attenuation end-member for the ice shell. Our calculations for the highly attenuating ice shell predict much lower frequencies, but these are likely questionable as they rely on an anelastic dispersion approximation that is only valid for a frequency-independent Q model. This correction is quite large for the low Q values in the highly attenuating model and they are extrapolated to very low frequencies comparable to the visco-elastic relaxation time of the ice shell, where constant Q is no longer a reasonable approximation. This is not likely to be a problem for the lower-attenuation model, however, as the frequencies are consistent to those predicted by a model with no attenuation. Excitation of this mode is, however, likely to be too small to measure, even with a surface installation. For example, the peak displacement of ${}_0S_2$ for a $M_W = 5$ event in the ice shell is on the order of a few μm. At the very low frequencies of this mode, this corresponds to accelerations of $\sim 10^{-12}$ m/s^2. This is approximately 3 orders of magnitude smaller than the noise level of a superconducting gravimeter [*Goodkind*, 1999] and several orders of magnitude smaller than the sensitivities of existing planetary instruments (Figure 4). In order for this mode to be measurable, we would either need to record a very large, and therefore unlikely, tectonic event or we would require another mechanism of excitation other than tectonic events in the ice shell.

[26] Determining the deeper thermal and chemical structure of the mantle is more problematic. In Paper 1, we obtained a range of models with different assumptions about the chemical composition of the mantle and core, as well as different proposed thermal profiles. When comparing the mode catalogs for these models, it is apparent that there are many modes that have significant sensitivity to these parameters, primarily through the perturbations in depths of transition between the core and mantle, and the mantle and ice-water layer (Figure 9). In general, these modes have frequencies lower than 0.01 Hz, and are in overtone mode branches. Unfortunately the ice-shell events only efficiently excite the fundamental mode branch, which has no significant sensitivity to composition below the ice shell, and thus these modes will not be observable for such an event. The fundamental mode branch does show some sensitivity to the thermal structure through the change in attenuation properties, but the details of this change are dependent on the precise temperature and pressure dependence of ice's seismic attenuation, which is poorly known.

[27] It is reasonable to expect that there will also be deeper events in the rocky mantle of Europa. Analogous events are observed in the Apollo data on the Earth's moon, and the evidence suggests that they are caused by tidal stressing [*Nakamura*, 1978]. While the tidal stresses in the rocky interior of Europa will be lower than those in the ice shell, there will likely be stresses of a similar order of magnitude as for the interior of Earth's moon, and so these

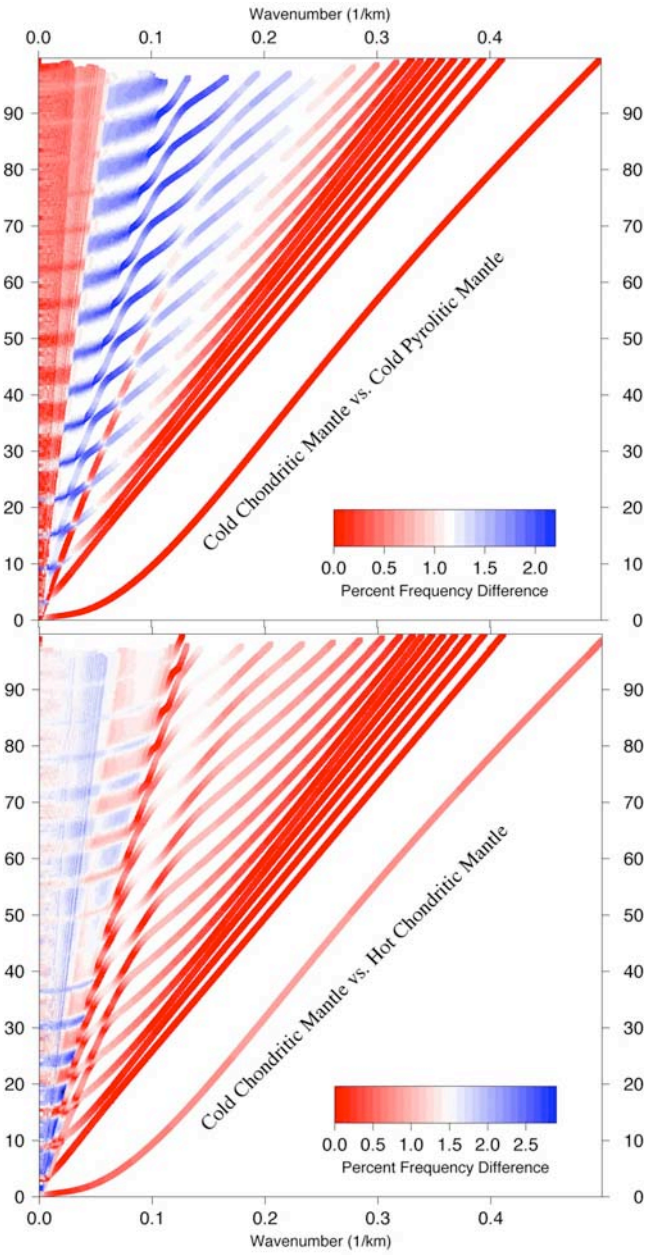

Figure 9. Modal frequency difference (%) as function of frequency and wave number for comparisons of (top) cold chondritic and pyrolitic models and (bottom) hot and cold chondritic models.

sources would excite modes with sensitivity to the deep structure of Europa. Unfortunately, the presence of an ice shell on top of a global liquid ocean means that seismic energy at depth is not well-coupled with the surface. For example, a candidate $M_W = 4$ event at 200 km depth (in the rocky mantle) produces seismic signals 4 to 5 orders of magnitude smaller than those observed from the candidate ice shell event described here. This suggests that it will be extremely difficult to measure usable seismic signals for deep events, and thus to determine the deep thermal and chemical structure of Europa or determine if the deep interior is tectonically active using such an approach.

7. Discussion

7.1. Differences From Surface Wave Observations on Earth

[28] It is interesting to note that many aspects of long-period seismology on Europa are very different from surface wave seismology on the Earth. Surface wave dispersion on the Earth, in general, is controlled by the depth-dependent velocity characteristics. Because of Earth's gravity, the pressure gradient causes a monotonic increase of velocity with depth, with some exceptions. This means that longer-period surface waves, which have greater sensitivity to deeper structure, are faster than shorter-period waves leading to characteristic seismograms with longer-period energy preceding shorter-period energy. On Europa, however, the lower gravity means that the pressure gradient is smaller, and seismic velocities are much closer to constant with respect to depth. Dispersion is introduced due to the physical properties of bending mode waves propagating in a shell of finite thickness. This means that longer-period waves are slower than shorter-period waves, producing seismograms with opposite characteristics than Earth seismograms. A similar signature is predicted for Love waves in an ice shell [*Kovach and Chyba*, 2001] and is observed at much higher frequencies in seismic measurements on terrestrial sea ice [*Crary*, 1955].

7.2. Effects of a Deep Surface Regolith and Scattering

[29] Several authors have proposed an extensive regolith in the top 1 km of the ice shell due to increased porosity and fractures from micro-impacts [*Nimmo et al.*, 2003; *Eluskiewicz*, 2004; *Nimmo and Schenk*, 2006; *Lee et al.*, 2005]. Depending on the length scale of these fractures, the regolith could potentially introduce strong scattering, which can lead to higher effective attenuation and extensive coda development. Additionally, such a layer would have markedly different velocities than the unfractured ice modeled in Paper 1. To test the effect of such a layer, we synthesized seismograms using a model with shear modulus reduced by a factor of 10 in the top kilometer, and $1/Q$, a measure of attenuation, increased by a factor of 4. For models with ice shells 10 km and thicker, this made little discernible difference to the dispersion curves, while for a 5 km thick shell, the changes were still relatively small (Figure 10). For a given seismic moment, the amplitudes of the surface wave were amplified on the order of 10%. For a given fault geometry, however, such a model will lead to decreased seismic amplitudes, as the seismic moment scales linearly with shear modulus in the source region. This would introduce a factor of 10 decrease in seismic moment for near-surface fractures.

[30] This approach, however, does not address the effect of strong scattering. On the Earth's moon, for example, both the short-period and long-period Apollo seismic data show codas with long duration which greatly reduce the amplitude of surface waves from spherical predictions [*Lognonné and Johnson*, 2006]. The frequency range for this effect, however, is primarily at periods shorter than 10 seconds. Modeling of the scattering on the moon suggests that it is

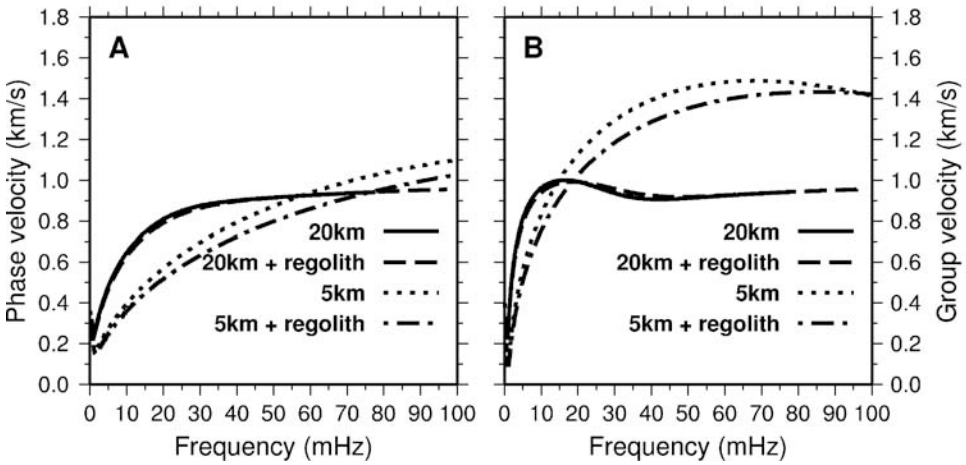

Figure 10. (a) Phase and (b) group velocity dispersion curves for models with 5 km and 20 km thick ice shells with and without a 1 km thick regolith layer. Changes to the dispersion for the thicker model are very small, while somewhat more pronounced for a thinner shell. Both cases are modeled for the highly attenuating ice shell end-member model.

due to a diffusive seismic energy regime in the upper ~20 km of the moon's regolith [*Dainty et al.*, 1974]. This regime is modeled as having scatterers with correlation length scales of a few kilometers in a region with very low intrinsic attenuation ($Q \sim 5000$). Other theoretical work on seismic scattering shows that the amplitudes of diffusive energy is only significant when scattering due to 3-D heterogeneity is large relative to intrinsic attenuation [*Wu*, 1985; *Zeng et al.*, 1991]. Such a scattering regime on Europa, however, would be constrained to a much shallower depth extent of no more than 2 or 3 kilometers as realistic thermal profiles suggest that at greater depths the ice will be approaching its melting point, and thus have significant intrinsic attenuation. Previous work has also shown that ice flow at this depth will remove all porosity [*Nimmo et al.*, 2003], removing the most likely candidate for pronounced seismic scatterers. The effect of scattering is also dependent on the ratio of the scale length of the scatterers to the wavelength of the seismic wave that is scattered [*Wu and Aki*, 1985]. The forward scattering coefficients increase exponentially with this ratio, the backscattering coefficients are peaked for ratios near 1, and both are several orders of magnitude smaller for a ratio of 0.1. For the case of the long-period Apollo data, which had peak sensitivity at 0.45 Hz, this ratio is near 1 for the modeled scatterers. However, the peak displacement amplitudes on Europa occur at periods longer than 200 seconds, and the observed fractures are at much smaller wavelengths. For acceleration data, on the other hand, the peak amplitudes do occur at the highest frequencies in our studied bandwidth, and it is reasonable to expect that these amplitudes could be greatly reduced by scattering effects, although that is highly dependent on the unknown 3-D structure on Europa.

7.3. Effects of Seismic Noise

[31] We do not have any estimate of the level of background seismic noise at Europa's surface. On the Earth, the seismic noise has characteristics that depend on the frequency band. The strongest noise is for periods from 6–12 seconds, and is related to excitation by the dominant period of wind-driven waves in the ocean interacting with shorelines. Such waves would not exist in Europa's ocean, and it is difficult to predict what kind of noise might be generated by a global sub-surface ocean where the wave excitation would presumably be dominantly in the tidal frequencies. One way to estimate the noise would be to assume many small opening crack events due to diurnal forcing, similar to those discussed by *Lee et al.* [2003]. The MFT measurements in Figure 7 include noise determined by 20 randomly distributed events on the planet surface with moment magnitudes between 2 and 3 with magnitudes defined by a Gutenberg-Richter distribution with a b-value of 1. This does not have a noticeable effect on the results, although a higher noise level could make measurements more difficult, requiring more advanced signal processing approaches.

[32] In the absence of larger events, however, such sources of systematic noise could be used as data, although it would likely require a surface installation of more than one sensor. The systematic noise, which would be scattered by inhomogeneities in the ice shell, could then be cross-correlated for station pairs to extract information about the surface wave propagation between the stations [e.g., *Campillo and Paul*, 2003].

7.4. Orbital-Based Measurements

[33] The synthetic seismograms presented here were calculated assuming a fixed receiver position. Unless an orbiter is at the correct altitude for geosynchronous orbit, however, the seismic measurements will be made at a moving point on the surface. This presents additional challenges. For example, an orbiter 100 km above the surface of Europa, a target orbit for several proposed missions to Europa, will have an orbital velocity relative to the surface that is comparable to the surface wave velocities. This will require careful processing, but may provide us with interesting methods for determining surface wave velocities from a single measurement.

[34] To test this, we adapted the mode summation code to synthesize seismograms at a moving observation point. For mode summation in 1-D models, this is a relatively simple

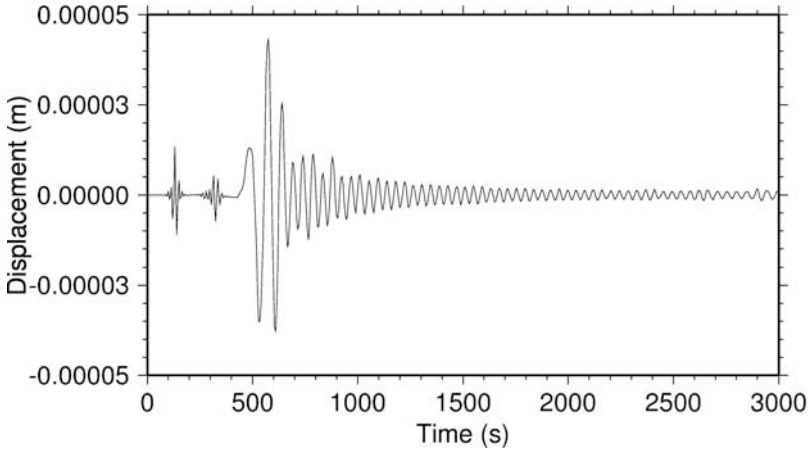

Figure 11. Three thousand seconds of seismic displacement (in m) for an observation point that starts 15° (410 km) east of the source at the event origin time and moves north with an apparent surface velocity of 1.4 km/s calculated in the low-attenuation 5 km thick ice shell model. The arrivals at about 120 s and 350 s are the P and S waves, respectively. Note the resonance at approximately 25 mHz following the first arriving surface wave energy at 500 s, which is a frequency band where the group velocity is comparable with velocity of the observation point.

modification. Following *Woodhouse and Girnius* [1982], we can write a mode summation seismogram for a fixed source and receiver configuration as

$$\mathbf{v} \cdot \mathbf{s} = \sum_{km} R_k^m(\theta_r, \phi_r) S_k^m(\theta_s, \phi_s) \exp(i\omega_k t), \tag{2}$$

where **v** is the instrument vector, which is a unit vector in the direction of motion sensed by the instrument which can also incorporate the instrument response, **s** is the elastic displacement field, k is a mode index which incorporates all degenerate mode singlets for given angular order l and radial order n, m is the azimuthal order of a mode singlet, and ω_k is the eigenfrequency of mode k. The amplitude of each mode singlet is determined by the source mechanism and the source-receiver geometry through the terms R_k^m and S_k^m, evaluated at the receiver and source coordinates, respectively. These can be expressed as

$$R_k^m(\theta_r, \phi_r) = \sum_{N=-1}^{1} R_{kN} Y_l^{Nm}(\theta_r, \phi_r) \tag{3}$$

$$S_k^m(\theta_s, \phi_s) = \sum_{N=-2}^{2} S_{kN} Y_l^{Nm}(\theta_s, \phi_s), \tag{4}$$

where Y_l^{Nm} are the generalized spherical harmonics of *Phinney and Burridge* [1973], and the coefficients R_{kN} and S_{kN} are defined by *Woodhouse and Girnius* [1982] in terms of the seismic moment tensor elements, the instrument response vector **v**, and the radial eigenfunctions of mode k. The location of the observation point only enters the expressions in the evaluation of the spherical harmonics term in (3). Therefore the seismogram at an observation point whose location is a known function of time can be calculated with a time-dependent R_k^m determined by evaluating the spherical harmonics term at each point in time at the appropriate location.

[35] While an exhaustive study on how best to extract useful measurements from such data has not yet been attempted, interesting observations are possible from simple inspection of the seismograms. For example, seismic displacement from an event that occurs near the trajectory of the orbiter recorded on an observation point moving away from the source location produces a seismogram at sufficient time after the event with a resonant frequency (Figure 11). This resonance is caused by a wave packet of a given frequency having a group velocity which closely matches the velocity of the observation point. Because the frequency at which the group velocity will match a given orbital velocity depends on the ice shell model, an observation of this resonance phenomenon may be diagnostic.

8. Conclusions

[36] Long-period seismic observations on Europa have potential to greatly expand our knowledge of the satellite. In particular, long-period displacement measurements with millimeter accuracy may be able to determine the current tectonic activity of Europa's surface, the presence of a liquid ocean, and the thickness of the ice shell. These observations hold considerable promise relative to shorter-period acceleration and velocity measurements, as the peak amplitudes occur at frequencies that minimize the complications from unknown 3-D heterogeneity and finite source dimension and duration. Such displacement measurements may be possible from orbit, but many instrument design and data processing details need to be carefully considered. Determination of deeper structure with seismic measurements is much more difficult in the presence of a global liquid subsurface ocean, which acts to decouple deeper seismic energy from the surface.

[37] **Acknowledgments.** This work was supported through the development of the Multiple Instrument Distributed Aperture Sensor (MIDAS; NASA grant NNG05GA25G) and NSF grant EAR-0308750. The manuscript benefited from reviews by Francis Nimmo, Philippe Lognonné, and an anonymous reviewer. This is contribution 06-12 of the Berkeley Seismological Laboratory.

References

Aki, K., and P. G. Richards (2002), *Quantitative Seismology*, 2nd ed., Univ. Sci. Books, Sausalito, Calif.

Anderson, G. D., G. Schubert, R. A. Jacobson, E. L. Lau, W. B. Moore, and W. L. Sjogren (1998), Europa's differentiated internal structure: Inferences from four Galileo encounters, *Science*, *281*, 2019–2022.

Billings, S. E., and S. A. Kattenhorn (2005), The great thickness debate: Ice shell thickness models for Europa and comparisons with estimates based on flexure at ridges, *Icarus*, *177*, 397–412.

Cammarano, F., V. Lekic, M. Manga, M. Panning, and B. Romanowicz (2007), Long-period seismology on Europa: 1. Physically consistent interior models, *J. Geophys. Res.*, doi:10.1029/2006JE002710, in press.

Campillo, M., and A. Paul (2003), Long-range correlations in the diffuse seismic coda, *Science*, *299*, 547–549.

Crary, A. P. (1955), A brief study of ice tremors, *Bull. Seismol. Soc. Am.*, *45*, 1–9.

Dainty, A. M., M. N. Toksöz, K. R. Anderson, P. J. Pines, Y. Nakamura, and G. Latham (1974), Seismic scattering and shallow structure of the moon in Oceanus Procellarum, *Moon*, *9*, 11–29.

Dziewonski, A., S. Bloch, and M. Landisman (1969), A technique for the analysis of transient seismic signals, *Bull. Seismol. Soc. Am.*, *59*, 417–444.

Eluskiewicz, J. (2004), Dim prospects for radar detection of Europa's ocean, *Icarus*, *170*, 234–236.

Geissler, P. E., et al. (1998), Evidence for non-synchronous rotation of Europa, *Nature*, *391*, 368–370.

Goodkind, J. M. (1999), The superconducting gravimeter, *Rev. Sci. Instrum.*, *70*, 4131–4152.

Greenberg, R., P. Geissler, G. Hoppa, B. R. Tufts, and D. D. Durda (1998), Tectonic processes on Europa: Tidal stresses, mechanical response, and visible features, *Icarus*, *135*, 64–78.

Hoppa, G., R. Greenberg, B. R. Tufts, P. Geissler, C. Phillips, and M. Milazzo (2000), Distribution of strike-slip faults on Europa, *J. Geophys. Res.*, *105*, 22,617–22,627.

Hoppa, G. V., B. R. Tufts, R. Greenberg, and P. E. Geissler (1999), Formation of cycloidal features on Europa, *Science*, *285*, 1899–1902.

Kivelson, M. G., et al. (2000), Galileo magnetometer measurements: A stronger case for a subsurface ocean at Europa, *Science*, *289*, 1340–1343.

Kovach, R. L., and C. F. Chyba (2001), Seismic detectability of a subsurface ocean on Europa, *Icarus*, *150*, 279–287.

Lammlein, D. (1977), Lunar seismicity and tectonics, *Phys. Earth Planet. Inter.*, *14*, 224–273.

Lee, S., M. Zanolin, A. M. Thode, R. T. Pappalardo, and N. C. Makris (2003), Probing Europa's interior with natural sound sources, *Icarus*, *165*, 144–167.

Lee, S., R. T. Pappalardo, and N. C. Makris (2005), Mechanics of tidally driven fractures in Europa's ice shell, *Icarus*, *177*, 367–379.

Leith, A. C., and W. B. McKinnon (1996), Is there evidence for polar wander on Europa?, *Icarus*, *120*, 387–398.

Lognonné, P., and C. Johnson (2006), Planetary seismology, *Treatise Geophys.*, in press.

Lognonné, P., and B. Mosser (1993), Planetary seismology, *Surv. Geophys.*, *14*, 239–302.

Lognonné, P., et al. (1998), The seismic OPTIMISM experiment, *Planet. Space Sci.*, *46*, 739–747.

Lognonné, P., et al. (2000), The NetLander very broad band seismometer, *Planet. Space Sci.*, *48*, 1289–1302.

McEwen, A. S. (1986), Tidal reorientation and the fracturing of Jupiter's moon Europa, *Nature*, *321*, 49–51.

Minshull, T. A., and N. R. Goulty (1988), The influence of tidal stresses on deep moonquake activity, *Phys. Earth Planet. Inter.*, *52*, 41–55.

Nakamura, Y. (1978), A1 Moonquakes: Source distribution and mechanisms, *Proc. Lunar Planet. Sci. Conf. 9th*, 389–399.

Nimmo, F., and P. Schenk (2006), Normal faulting on Europa: Implications for ice shell properties, *J. Struct. Geol.*, *28*, 2194–2203.

Nimmo, F., R. T. Pappalardo, and B. Giese (2003), On the origins of band topography, Europa, *Icarus*, *166*, 21–32.

Pappalardo, R. T., et al. (1999), Does Europa have a subsurface ocean? Evaluation of the geological evidence, *J. Geophys. Res.*, *104*, 24,015–24,055.

Pasyanos, M. E., D. Dreger, and B. Romanowicz (1996), Towards real-time estimation of regional moment tensors, *Bull. Seismol. Soc. Am.*, *86*, 1255–1269.

Pedersen, H. A., O. Coutant, A. Deschamps, M. Soulage, and N. Cotte (2003), Measuring surface wave phase velocities beneath small broadband arrays: Tests of an improved algorithm an application to the French Alps, *Geophys. J. Int.*, *154*, 903–912.

Phinney, R. A., and R. Burridge (1973), Representations of the elastic-gravitational excitation of a spherical Earth model by generalized spherical harmonics, *Geophys. J.R. Astron. Soc.*, *34*, 451–487.

Press, F., and M. Ewing (1951), Propagation of elastic waves in a floating ice sheet, *Eos Trans. AGU*, *32*, 673–679.

Ruiz, J. (2005), The heat flow of Europa, *Icarus*, *177*, 438–446.

Sarid, A. R., R. Greenberg, G. V. Hoppa, T. A. Hurford, B. R. Tufts, and P. Geissler (2002), Polar wander and surface convergence of Europa's ice shell: Evidence from a survey of strike-slip displacement, *Icarus*, *158*, 24–41.

Schenk, P. M., and W. B. McKinnon (1989), Fault offsets and lateral crustal movement on Europa: Evidence for a mobile ice shell, *Icarus*, *79*, 75–100.

Woodhouse, J. H. (1988), The calculation of eigenfrequencies and eigenfunctions of the free oscillations of the Earth and the Sun, in *Seismological Algorithms*, pp. 321–370, edited by D. J. Doornbos, Elsevier, New York.

Woodhouse, J. H., and T. P. Girnius (1982), Surface waves and free oscillations in a regionalized Earth model, *Geophys. J.R. Astron. Soc.*, *68*, 653–673.

Wu, R. S. (1985), Multiple scattering and energy transfer of seismic waves—Separation of scattering effect from intrinsic attenuation—I. Theoretical modelling, *Geophys. J.R. Astron. Soc.*, *82*, 57–80.

Wu, R. S., and K. Aki (1985), Elastic wave scattering by a random medium and the small-scale inhomogeneities in the lithosphere, *J. Geophys. Res.*, *90*, 10,261–10,273.

Zahnle, K., P. Schenk, H. Levison, and L. Dones (2003), Cratering rates in the outer solar system, *Icarus*, *163*, 263–289.

Zeng, Y., F. Su, and K. Aki (1991), Scattering wave energy propagation in a random isotropic scattering medium: 1. Theory, *J. Geophys. Res.*, *96*(B1), 607–619.

F. Cammarano, V. Lekic, and B. Romanowicz, Berkeley Seismological Laboratory, University of California, Berkeley, 215 McCone Hall, Berkeley, CA 94720, USA.

M. Manga, Department of Earth and Planetary Science, University of California, Berkeley, Berkeley, CA 94720, USA.

M. Panning, Department of Geosciences, Princeton University, 318 Guyot Hall, Princeton, NJ 08544, USA. (mpanning@princeton.edu)